University of Pennsylvania
ScholarlyCommons

Departmental Papers (MEAM)

Department of Mechanical Engineering & Applied Mechanics

January 2007

Induction and measurement of minute flow rates through nanopipes

Shashank Sinha
University of Pennsylvania

Maria Pia Rossi
Drexel University

D. Mattia
Drexel University

Yury Gogotsi
Drexel University

Haim H. Bau
University of Pennsylvania, bau@seas.upenn.edu

Follow this and additional works at: http://repository.upenn.edu/meam_papers

Recommended Citation

Sinha, Shashank; Rossi, Maria Pia; Mattia, D.; Gogotsi, Yury; and Bau, Haim H., "Induction and measurement of minute flow rates through nanopipes" (2007). *Departmental Papers (MEAM)*. 79.
http://repository.upenn.edu/meam_papers/79

Reprinted in *Physics of Fluids*, Volume 19, Issue 1, January 2007, Article 013603, 8 pages.
Publisher URL: http://dx.doi.org/10.1063/1.2432914

This paper is posted at ScholarlyCommons. http://repository.upenn.edu/meam_papers/79
For more information, please contact libraryrepository@pobox.upenn.edu.

Induction and measurement of minute flow rates through nanopipes

Abstract
A simple technique to simultaneously induce fluid flow through an individual nanopipe and measure the flow rate and the pressure difference across the pipe is described. Two liquid drops of different sizes are positioned at the two ends of the nanopipe. Due to the higher capillary pressure of the smaller drop, flow is driven from the smaller drop to the bigger drop. The instantaneous pressures of the two drops are estimated from the drops' shapes and sizes. The flow rate is estimated by monitoring the sizes of the drops as functions of time with a microscope and a video camera. A theory that correlates the drops' sizes and the flow rate is derived. Measurements are carried out with an ionic salt and glycerin to estimate the effective tube radius of the nanopipes with diameters ranging from 200 to 300 nm. The tubes' diameters are independently measured with a scanning electron microscope. The method is also verified by tracking the motion of fluorescent particles through the nanopipe. The paper provides a simple technique for studying extremely low flow rates in nanofluidic systems. When working with low-evaporation fluids such as ionic salts, the measurements can be carried out with an electron microscope.

Keywords
pipe flow; drops; capillarity; flow measurement

Comments
Reprinted in *Physics of Fluids*, Volume 19, Issue 1, January 2007, Article 013603, 8 pages.
Publisher URL: http://dx.doi.org/10.1063/1.2432914

This journal article is available at ScholarlyCommons: http://repository.upenn.edu/meam_papers/79

Induction and measurement of minute flow rates through nanopipes

Shashank Sinha
Department of Mechanical Engineering & Applied Mechanics, University of Pennsylvania, Philadelphia, Pennsylvania 19104

Maria Pia Rossi, D. Mattia, and Yury Gogotsi
Department of Material Science and Engineering and A. J. Drexel Nanotechnology Institute, Drexel University, Philadelphia, Pennsylvania 19104

Haim H. Bau[a)]
Department of Mechanical Engineering & Applied Mechanics, University of Pennsylvania, Philadelphia, Pennsylvania 19104

(Received 19 September 2006; accepted 12 December 2006; published online 25 January 2007)

A simple technique to simultaneously induce fluid flow through an individual nanopipe and measure the flow rate and the pressure difference across the pipe is described. Two liquid drops of different sizes are positioned at the two ends of the nanopipe. Due to the higher capillary pressure of the smaller drop, flow is driven from the smaller drop to the bigger drop. The instantaneous pressures of the two drops are estimated from the drops' shapes and sizes. The flow rate is estimated by monitoring the sizes of the drops as functions of time with a microscope and a video camera. A theory that correlates the drops' sizes and the flow rate is derived. Measurements are carried out with an ionic salt and glycerin to estimate the effective tube radius of the nanopipes with diameters ranging from 200 to 300 nm. The tubes' diameters are independently measured with a scanning electron microscope. The method is also verified by tracking the motion of fluorescent particles through the nanopipe. The paper provides a simple technique for studying extremely low flow rates in nanofluidic systems. When working with low-evaporation fluids such as ionic salts, the measurements can be carried out with an electron microscope. © *2007 American Institute of Physics*. [DOI: 10.1063/1.2432914]

I. INTRODUCTION

Studies of the dependence of the flow rate of various fluids through minute conduits on the pressure drop across these conduits have been of interest since the pioneering work of Poiseuille[1] about 160 years ago. Poiseuille carried out his experiments in tubes with diameters of tens of micrometers. Analysis of Poiseuille's experimental data provides surprisingly accurate estimates of water's viscosity at various temperatures.[2] More recently, researchers shifted to investigating fluid flow in nanometer-sized conduits. In particular, there has been a growing interest in determining whether and under what conditions fluid flow exhibits slip along solid walls. Most slip flow phenomena have been observed along hydrophobic surfaces, typically surfaces coated with a self-assembled monolayer (SAM).[3–10] The reported values of slip lengths range widely from a few nanometers to a few micrometers and were also found to be a function of the shear rate.[11] Slip effects are most pronounced in nanosize tubes. Recently, Majumdar *et al.*[12] reported that various fluids exhibited surprisingly high flow rates, 4–5 orders of magnitude larger than theoretical predictions with corresponding slip lengths of 3–70 μm, in membranes consisting of very large numbers of multiwalled carbon nanotubes (MWNT) of inner diameters of ~7 nm. Holt *et al.*[13] observed a similar behavior in the case of a bundle of sub-2 nanometer diameter nanotubes. In both cases, the analysis and verification of the data is complicated by the fact that the measured flow rates constitute an average over a large number of tubes, possibly with a range of diameters and because of concerns about possible flow along the tubes' outer surface. Clearly, it would be desirable to measure flow rates through individual nanotubes.

In this paper, we present a simple technique to induce liquid flow through a single nanopipe while at the same time allowing for the estimation of the pressure drop across the tube and the flow rate through the tube. The method consists of positioning two drops of different sizes at the two ends of a tube. Since the pressure of the liquid in the smaller drop is larger than in the bigger drop, liquid will flow from the smaller drop to the bigger one. The liquid flow rate is estimated by monitoring the sizes of the drops. The instantaneous pressures in the drops are estimated from the drops' radii of curvature. We describe the relevant theory and carry out a few experiments to validate the theory.

II. THEORY

The experimental setup consists of a nanopipe located on a flat substrate. Two liquid drops of different sizes are placed at the two ends of the nanopipe (Fig. 1). The drops wet the substrate material. We assume that the drops form approximately spherical cap shapes. The base radii of the drops are denoted R_1 and R_2 and the heights of the drops are denoted

[a)]Author to whom correspondence should be addressed.

 © 2007 American Institute of Physics

Downloaded 14 Mar 2007 to 165.123.34.86. Redistribution subject to AIP license or copyright, see http://pof.aip.org/pof/copyright.jsp

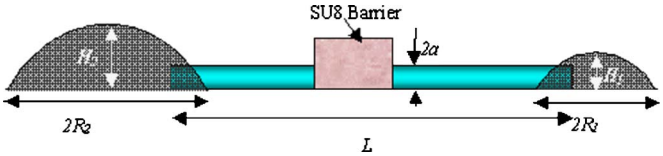

FIG. 1. A schematic depiction of the experimental set-up—a nanopipe with two drops placed at its ends and SU8 barrier in the middle.

H_1 and H_2. The drops form contact angle $\theta < 90°$ with the substrate. A barrier positioned transverse to the nanotube precludes fluid flow along the outside surface of the tube.

The volume (V) of each drop $(\pi/6)(3R^2+H^2)H$ is rewritten in terms of the contact angle (θ) as $V=(\pi/6)R^3S$, where $S=[3+((1-\cos\theta)/\sin\theta)^2][(1-\cos\theta)/\sin\theta]$. The corresponding surface area of the drop that is exposed to the air is $A=2\pi(RH/\sin\theta)=2\pi R^2B$, where $B=(1-\cos\theta)/\sin\theta$. The pressure inside the drop above the atmospheric pressure is $(2\sigma\sin\theta/R)$, where σ is the surface tension of the liquid. The drop's capillary pressure increases significantly as its size decreases. For example, when a drop of $R\sim 1$ μm is placed at one end of the tube, the excess pressure inside the drop is about one atmosphere. When the other end of a 10 μm long nanopipe is in contact with a large drop or a flat film of liquid, the pressure gradient along the tube is $\sim$10 GPa/m. Due to the tube's small size, the flow inside the tube remains laminar even in the presence of this extraordinarily high pressure-gradient. Typically, the ratio between the tube's length and diameter is larger than 30, the velocities are on the order of 1 μm/s, and the Reynolds number is 10^{-6} or smaller. Thus, entry length effects can be neglected and the flow through the entire length of the tube can be assumed to be fully developed. The flow rate of fully developed, Poiseuille flow is $[\pi a^4/(8\mu)](\Delta P/L)$, where a is the tube's radius, μ is the fluid's viscosity, L is the nanotube's length, and ΔP is the pressure drop across the tube's length.

Experiments were carried out with an ionic liquid that has an insignificant rate of evaporation and with glycerin. In the latter case, evaporation was of concern and was accounted for in our theory. The rate of volumetric change due to evaporation can be expressed in the form $dV/dt=-\pi\alpha_e SR/2$, where α_e is an empirically determined coefficient. In the above, we assume that the relative humidity of the surrounding air is sufficiently low to preclude condensation.

The pressure difference between the two drops is $2\sigma\sin\theta(1/R_1-1/R_2)$. The rate of mass loss in the smaller drop is equal to the rate of mass gain by the bigger drop minus evaporation losses.

$$\frac{\pi}{2}\rho_l R_1^2 S dR_1 = -\frac{\pi\rho_l a^4}{8\mu}\frac{2\sigma\sin\theta}{L}\left(\frac{1}{R_1}-\frac{1}{R_2}\right)dt - \frac{\pi}{2}\alpha_e\rho_l S R_1 dt \tag{1}$$

and

$$\frac{\pi}{2}\rho_l R_2^2 S dR_2 = \frac{\pi\rho_l a^4}{8\mu}\frac{2\sigma\sin\theta}{L}\left(\frac{1}{R_1}-\frac{1}{R_2}\right)dt - \frac{\pi}{2}\alpha_e\rho_l S R_2 dt. \tag{2}$$

The last terms in Eqs. (1) and (2) correspond to mass loss due to evaporation. The above theory is applicable only when $R_i > a$.

Equations (1) and (2) constitute a set of coupled, first-order, ordinary differential equations for R_1 and R_2 with the initial conditions $R_1(0)=R_{1,0}$ and $R_2(0)=R_{2,0}$. These equations can be readily integrated numerically. Analytic solutions can be obtained in some limiting cases.

When $R_2 \gg R_1$ (and neglecting evaporation), we can assume that R_2 remains approximately constant throughout the process. Integrating Eq. (1), we obtain

$$R_2^4\ln\left(\frac{R_2-R_1}{R_2-R_{1,0}}\right) - 3R_2^3(R_{1,0}-R_1) + \frac{3}{2}R_2^2[(R_2-R_1)^2 - (R_2-R_{1,0})^2] - \frac{R_2}{3}[(R_2-R_1)^3-(R_2-R_{1,0})^3] = -\frac{a^4}{8\eta S}\left(\frac{2\sigma\sin\theta}{L}\right)t. \tag{3}$$

When $R_2\to\infty$ (i.e., when the larger drop is replaced with a liquid film) and neglecting evaporation, Eq. (3) can be further simplified to

$$\left(\frac{R_1(t)}{R_{1,0}}\right)^4 = 1-\left(\frac{a}{R_{1,0}}\right)^4\frac{2\sin\theta}{S}\frac{t}{\tau}, \tag{4}$$

where $\tau=\mu L/\sigma$ is the time constant. By plotting the fourth power of the radius of the smaller drop as a function of time, one can estimate either the tube's radius (a) when the fluid's thermophysical properties are known, or the effective liquid viscosity (μ) when the tube's radius is known.

III. MATERIALS

The experiments were carried out with carbon nanopipes grown by chemical vapor deposition at 670 °C in an alumina template.[14] These tubes had amorphous carbon walls and are referred to as 670 °C tubes. Some of the tubes were subsequently annealed in an inert atmosphere at 1850 and 2000 °C. During the annealing process, the carbon in the tubes' walls graphitized to form structures that resemble multiwalled carbon nanotubes. We refer to the graphitized, annealed tubes according to their annealing temperature as 1850 and 2000 °C tubes. The annealing reduced the surface energy and the wettability of the tubes. For example, the 670 and 2000 °C tubes had, respectively, contact angles of 44° and 77° with water.[15,16] The tubes had a nominal diameter of 200–300 nm and a wall thickness of about 15 nm. The actual diameters of the tubes varied and were measured with a scanning electron microscope (SEM). Previously, Kim *et al.* studied the filling of similar tubes with various liquids[17] and with particles.[18]

For improved contrast, experiments were carried out on a substrate consisting of a gold layer evaporated on a glass

Downloaded 14 Mar 2007 to 165.123.34.86. Redistribution subject to AIP license or copyright, see http://pof.aip.org/pof/copyright.jsp

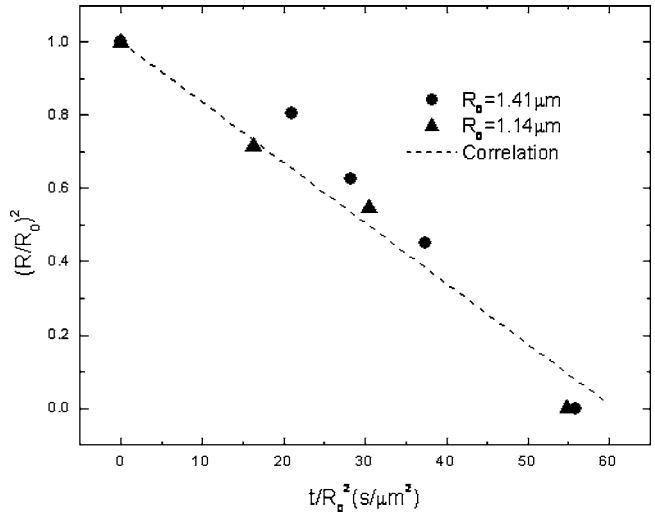

FIG. 2. The radius of the evaporating glycerin drop as a function of time at room temperature (22 °C). The symbols correspond to experimental data and the solid line to the correlation $R^2=R_0^2-\alpha_e t$, where $\alpha_e \sim 1.65 \times 10^{-14}$ m²/s.

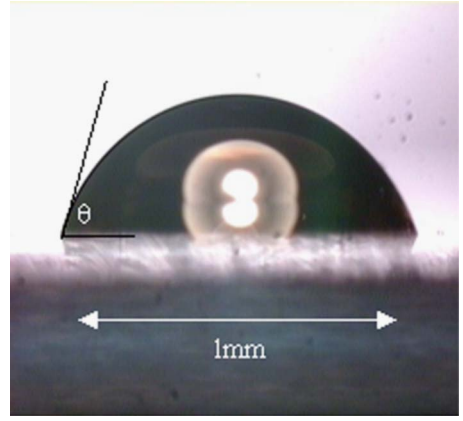

FIG. 3. The contact angle of a glycerin drop on a gold surface.

slide. An alcohol drop, containing a dilute solution of carbon pipes, was placed on top of the gold surface and allowed to evaporate, leaving a dispersion of nanotubes on the surface. The tubes adhered to the surface through van der Waals interactions. AFM measurements suggest that the tubes sagged slightly, assuming an elliptical cross section with their horizontal diameter being slightly larger than the vertical one.

To prevent liquid flow in the wedge formed between the tube and the substrate, a barrier made of negative photoresist (SU-8 2005, Microchem Inc.) was placed transverse to the tube as shown schematically in Fig. 1 and in the photograph in Fig. 6. The negative resist was administered with a glass micropipette. The micropipette was formed by pulling the tip of a capillary tube (nominal outer diameter of 0.7 mm) down to a 1–2 μm diameter with a glass puller (Sutter P2000). The micropipette was connected to a syringe through a flexible tube and placed in a glass tube holder mounted on a three-axis, hydraulic micromanipulator (Narishige MWS2). The syringe pressurized the micropipette to eject SU8 at its narrow end. As the SU8 ejected from the micropipette's end, the micropipette was traversed perpendicular to the nanotube to form a few-micrometer-wide barrier. Subsequently, the SU8 barrier was exposed to a mercury arc UV lamp for 5 min, followed by a 1 min heating at 70–80 °C on a hotplate. The SU8 solidified when cooled to room temperature and prevented any liquid flow along the outer surface of the nanopipe.

Experiments were carried out with ionic salt (Fluka 04365; i.e., 1-ethyl-3-methyl-imidazolium from sigmaaldrich.com) and with glycerin (96% purity from PTI process chemicals). The ionic salt did not exhibit any evaporation. Ionic slat drops were observed for days without any measurable change in their size. Unfortunately, the same was not true with the glycerin. To estimate the rate of evaporation of glycerin drops, we placed the drops on gold surfaces and monitored their sizes as functions of time at 22 °C. Figure 2 depicts the variation of the drop radius due to evaporation alone. The radius of the drop (R) as a function of time correlated well with a formula of the form $R^2=R_0^2-\alpha_e t$, where $\alpha_e \sim 1.65 \times 10^{-14}$ m²/s.

Using the above correlation, we estimate the fraction of the drop's mass lost by evaporation (when $t_{\text{total}} \ll t_{\text{ev}}$) as

$$\frac{\Delta m_{\text{evaporation}}}{m_{\text{drop}}} = 1.2\frac{t_{\text{total}}}{t_{\text{ev}}}. \tag{5}$$

In the above, t_{total} is the time needed for the drop to completely disappear due to both flow through the nanotube and evaporation. t_{total} is a function of the tube's diameter. t_{ev} is the time needed for the drop to disappear by evaporation alone. When $R_2 \to \infty$, $t_{\text{total}}/t_{\text{ev}}$ ranged from 0.01 to 0.1, depending on the initial size of the drop. The smaller the initial size, the faster the flow rate and the smaller the amount of time that is available for evaporation. Hence, $t_{\text{total}}/t_{\text{ev}}$ increased as the initial drop size was increased. For example, when $R_{1,0}=1.22$ μm, $t_{\text{total}}/t_{\text{ev}} \sim 0.02$ and when $R_{1,0}=2.8$ μm, $t_{\text{total}}/t_{\text{ev}} \sim 0.11$. The corresponding mass fractions lost to evaporation [Eq. (4)] were, respectively, 0.02 and 0.13 when $R_{1,0}=1.22$ and 2.8 μm. When the initial drop size was ≤ 1 μm, we neglected evaporative losses.

The static contact angle of the glycerin with the gold surface was estimated by taking a side image of a millimeter-size drop with a high-resolution Nikon digital camera equipped with a macro lens and bellow setup (Fig. 3). The height and the base's diameter were measured for a few drops to yield a static contact angle of 66±3°. Similar measurements of the ionic liquid's contact angle with the glass surface yielded a contact angle of 56±4° and with the gold surface, 52±4°.

In the actual experiments, the presence of the nanotube may have caused small contact angle nonuniformities along the micrometer-size drop's perimeter due to the liquid wetting the tube's material.[16] Furthermore, in the presence of fluid flow, the magnitude of the contact angle decreased slightly since the receding contact angle is generally smaller than the static contact angle. The above effects were not included in our analysis. We note, however, that a 6% error in contact angle would affect our estimate of the tube's radius a by about 2% and the estimate of the effective viscosity (μ) by ~9%.

Downloaded 14 Mar 2007 to 165.123.34.86. Redistribution subject to AIP license or copyright, see http://pof.aip.org/pof/copyright.jsp

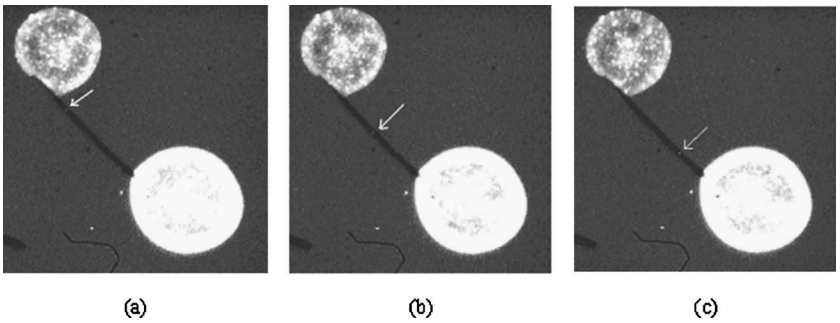

FIG. 4. The position of the fluorescent particle inside the nanotube as liquid flows from the smaller drop to the bigger drop. The arrow indicates the location of the particle in snapshots taken at (a) $t=0$ s, (b) $t=3.7$ s, and (c) $t=8.2$ s.

The surface tension and viscosity of the glycerin (96% purity) are, respectively, $\sigma=63.1$ mN/m and $\mu=486.8$ mPa s at $T=24$ °C. The corresponding properties of the ionic liquid (Fluka 04365, 1-ethyl-3-methylimidazolium) were obtained by in-house measurements. The surface tension was estimated from the equilibrium level in a glass capillary tube to be 0.042 N/m. The kinematic viscosity (available from manufacturer's data sheet) is 34×10^{-6} m^2/s, and the specific gravity is 1.24 at room temperature.

IV. EXPERIMENTAL PROCEDURE

All the experiments were carried out under an Olympus inverted microscope. A glass micropipette (produced as described above) was filled with ionic liquid or glycerin by capillarity suction. Subsequently, the micropipette was connected to a syringe through a flexible tube and fixed in the holder of the Narishige micromanipulator. The micropipette was transversed toward the surface at a 10° inclination until its tip made contact with the surface. When the tip touched the substrate, liquid film formed beneath the pipette and a drop was left as the micropipette moved away from the surface. The size of the drop was controlled by adjusting the pressure with the syringe pump. When the drop/film touched the end of the nanotube, the liquid filled the carbon nanotube by capillary suction.

Two different types of experiments were carried out. In one set of experiments, a drop was placed at one end of the nanotube. Then, the micropipette was brought near the other end of the nanopipe and deposited a thin liquid film beneath the micropipette. The micropipette was moved slowly using the nanomanipulator until the liquid film touched the nanotube's end. Since the nanotube was filled with liquid, the higher pressure in the drop drove liquid flow from the drop into the film. In the second set of experiments, a drop with a diameter of 3–10 μm was placed at one end of the tube and a smaller drop at the other end of the tube. The length of the nanopipe was measured with the microscope's reticle.

During the experiments, the drops were recorded at magnifications ranging from 400X to 1000X with a video camera (Sony camcorder, DCR PC3200 and Watec 120N) that was mounted on top of an upright microscope (Olympus BX51). The liquid drops' radii were estimated using the tube's length as a reference. The base of each drop formed an elliptic shape. Both major and minor half-axes $R_{\|}$ and $R_{\perp}$ of the base were measured as functions of time, and the arithmetic average radius $R=(R_{\|}+R_{\perp})/2$ was calculated. Typically, $|R_{\|}-R_{\perp}|<0.25R$.

To verify that the theoretical predictions provide a reasonable estimate of the flow velocity, we seeded the fluid with fluorescent tracer particles and monitored their velocity. The fluorescent particles were visible through the tube's wall. Fluorescent yellow particles (Spherotech Inc.) of 40–60 nm diameters were mixed with glycerin [1 part particle solution (1% w/v) in 100 parts of glycerin]. The smaller drop was laden with tracer particles. Due to the high dilution, only a few particles were present inside the tube at any time. As the suspension translocated through the tube, the fluorescence was excited with a mercury lamp and the resulting emission was observed through the thin wall of the nanotube. The particles' motion was monitored with the optical microscope at 1000X magnification and recorded with a high sensitivity CCD camera (Watec 120N). The camera was set to 1/4 seconds exposure to obtain sufficient integration time to facilitate the visualization of a single fluorescent particle inside the nanotube. Due to the long exposure time, meaningful data could be obtained only at very slow flow rates. To achieve the necessary low flow rates, we used the two-drop method with drops of similar initial sizes. When we placed two liquid drops with average radii of 7.2 and 9.8 μm, we obtained an initial average flow velocity of 1.3 μm/s, which could be readily discerned with the above exposure time. Due to the large drop sizes, evaporation was significant. Since the change in the drop sizes was insignificant during the course of the velocity measurement, we estimated the pressure difference and the flow velocity based on the instantaneous drop sizes. In this calculation, we used a tube with a known diameter. In order to allow uninterrupted observation of the particles, we did not erect the transverse barrier in these experiments.

Figure 4 features a sequence of photographs taken in the course of the experiment. The location of the fluorescent particle at various instants in time is indicated with an arrow. In the course of its motion along the tube, due to Brownian motion, the particle migrated in and out of focus. The particle's velocity was estimated based on the distance covered by the particle between subsequent snapshots. The fluid velocity could be assumed to be nearly constant during the residence time of the particle inside the tube.

Figure 5 depicts the measured velocities of the three particles (▲,■ and ●) as functions of time. The dashed line is

Downloaded 14 Mar 2007 to 165.123.34.86. Redistribution subject to AIP license or copyright, see http://pof.aip.org/pof/copyright.jsp

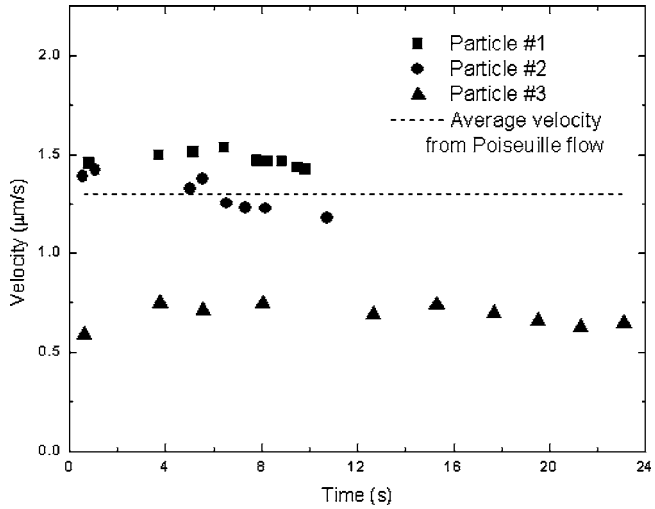

FIG. 5. The symbols and the dashed line depict, respectively, the measured velocity of the particles and the predicted velocity [Eq. (1)] as functions of time. The nanotube diameter is ~300 nm.

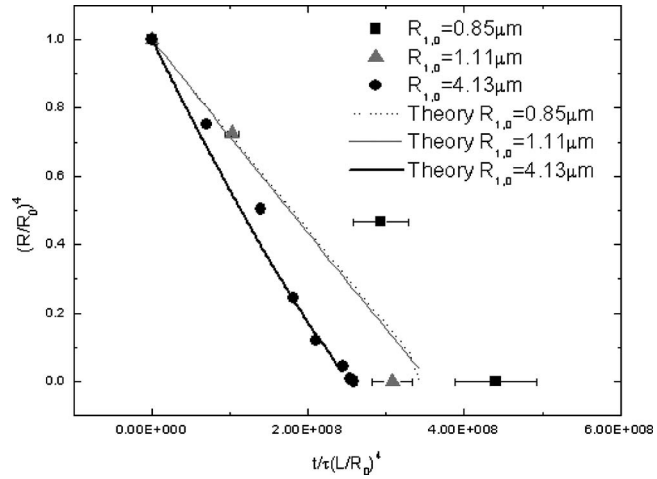

FIG. 7. The drop radius as a function with time for a 670 °C nanotube in a single drop experiment. The working fluid is glycerin. The symbols and lines correspond, respectively, to experimental data and theoretical predictions.

the theoretical prediction, obtained from Eq. (1), for the cross-sectionally averaged fluid velocity. Since the radial location of the particles is not known, we did not attempt to predict the particles' velocities. Based on Happel and Brenner[19] (Eq. 7–3.24), a particle of the size used here and located at the tube's center will translocate at nearly the maximum fluid velocity (~$1.96U$, where U is the cross-sectionally averaged velocity). Thus, depending on the radial location of the particle, its velocity will range from zero to nearly the fluid's maximum velocity. Witness that the particles' velocities are always below the maximum velocity that corresponds to Poiseuille flow (twice the average velocity). In two of the experiments, the particles' velocities were close to the predicted, average velocity. In the third experiment, the velocity was about half the average velocity. We speculate that in the latter case, the particle may have translocated in close vicinity to the wall where the velocity was lower. Particle-wall interactions may have also played a role in slowing the particle's migration speed. Although Brownian motion might have had a significant effect on the radial location of the particle, it did not play a significant role in the axial motion. Using the Stokes-Einstein equation, we estimate the Peclet number based on the particle's diameter to be 2.8. In other words, even in the presence of a concentration gradient of particles, the ratio of the diffusion and convection times needed to transverse the length of the tube would be greater than 200. In our case, since we are tracking individual particles, there is even less of a concern that Brownian motion affects the particle's velocity measurement since there should be no Brownian contribution to the net displacement.

V. RESULTS

We carried out a sequence of experiments with the single and double drop techniques. In each case, we estimated the tubes' radii and compared the estimated values with values obtained with SEM measurements.

Figures 6 and 7 describe the experiments with the single drop technique. The working fluid is glycerin. Figure 6 consists of snapshots of the experiment at different time instances. The glycerin drop at the upper end of the nanopipe is sucked into the thin film that formed under the micropipette at the other end. The initial radius of the drop is $R_{1,0}=2.96$ μm. As time passes, the size of the drop decreases until, after 18 s, the drop has completely disappeared.

Figure 7 depicts the fourth power of the measured, average base radius (R_1) of the glycerin drop as a function of time (t). The drop's radius is normalized with the initial radius $R_{1,0}$, and the time is normalized with the time constant $\tau=\mu L/\sigma$. For glycerin at room temperature, $\tau=0.13$ ms. The drop is in contact with one end of a 670 °C nanotube. The other side of the tube is in contact with a liquid film (see Fig. 6). The various symbols correspond to various initial radii of the drop's base: $R_{1,0}=0.85$ μm (■), 1.11 μm (▲), and

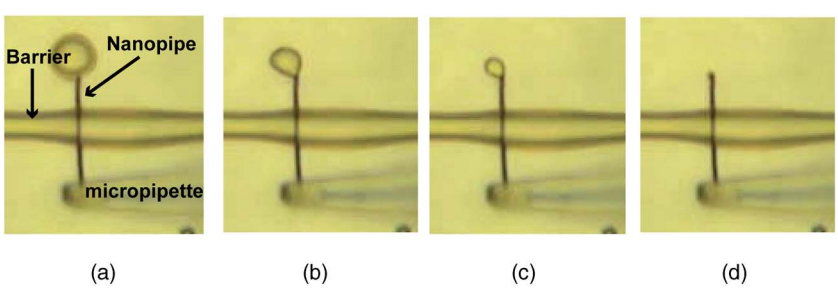

FIG. 6. Images depicting the experiment at various instants in time. (a) $t=0$ s; (b) $t=14$ s; (c) $t=16$ s; and (d) $t=18$ s. The working fluid is glycerin. The initial radius of the drop is $R_{1,0}=2.96$ μm.

Downloaded 14 Mar 2007 to 165.123.34.86. Redistribution subject to AIP license or copyright, see http://pof.aip.org/pof/copyright.jsp

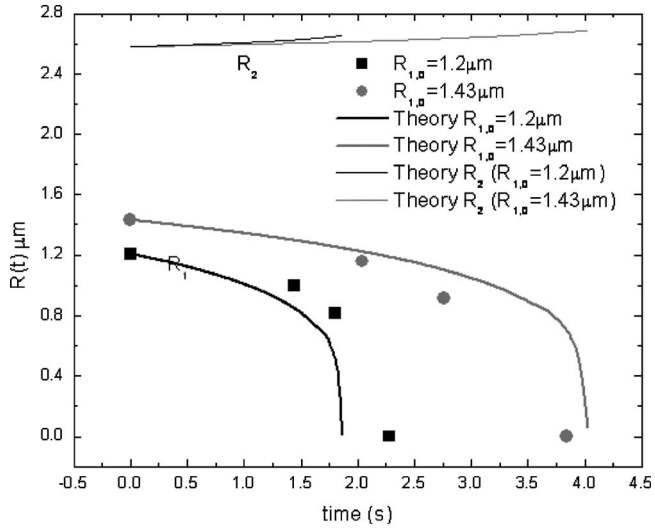

FIG. 8. Double drop experiment. The radii of the smaller drops R_1 are depicted as functions of time. Solid lines correspond to theoretical predictions. The dashed lines at the top of the figure depict R_2 as a function of time. The working fluid is glycerin.

4.13 μm (●). Except for the case of $R_{1,0}$=4.13 μm, the drops vanished within 1 s, and it was possible to obtain only two or three data points. Errors in the measurements of the radii of the smaller size drops (i.e., $R_{1,0}$=0.85 μm) and the short time available for measurement gave rise to significant uncertainty, which is shown with horizontal bars in the figure.

The tube's radius (a) was estimated by seeking the "a" value that minimized the discrepancy E between the computed (R_{com}) and measured (R_m) radii, where $E(a)=\Sigma_{i=1}^{N}\int_0^{t_{\text{total}}}[R_{\text{com},i}(t;a)-R_{m,i}(t)]^2dt$ and N is the number of independent measurements carried out with the same tube. The theoretical $R_{\text{com}}(t)$ was computed by specifying a value for a and solving Eq. (1) numerically (accounting for evaporation) with the variable order Adams-Bashforth-Moulton multistep solver. The value of a was adjusted until E was minimized. The theoretical curves with the best a=131 nm are depicted with dotted (R_{10}=0.85 μm), light solid (R_{10} =1.11 μm), and heavy solid (R_{10}=4.13 μm) lines. Witness that when $R_{1,0}$=1.11 and 4.13 μm, $(R/R_0)^4$ decreases nearly linearly as a function of time with an approximate slope of $-2\sigma a^4 \sin\theta/S\mu L$ in agreement with Eq. (4).

Similar experiments were carried out with the double drop technique. The double drop technique allowed better control of the process. By placing two drops of similar size, one can maintain an initial small pressure difference between the two drops with a resulting small flow rate. The disadvantage is that in the case of volatile fluids, evaporation may play a prominent role.

Figure 8 depicts a sample of the results of the double drop experiment. The working fluid is glycerin. In these experiments, R_2 was sufficiently large and remained nearly constant throughout the experiment. The dashed lines at the top of Fig. 8 depict R_2 as a function of time. Witness that R_2 changed by less than 5% throughout the experiment. Consequently, in the theoretical calculation, we assumed that $R_2 \sim R_{2,0}$ remained constant. Figure 8 depicts R_1 as a function of time when $R_{1,0}$=1.2 μm (■) and 1.43 μm (●). The solid lines correspond to theoretical estimates of the radius obtained by numerically solving Eq. (1) for R_1 as a function of t. The optimal value of the tube's radius a was determined by minimizing the discrepancy $E(a)$ between the theoretical prediction and the experimental data and found to be 131 nm.

Numerous experiments with the single and double drop techniques were carried out both with ionic liquid (Fluka 04365, 1-ethyl-3-methyl-imidazolium) and with glycerin. In each case, the tube's radius was estimated using the method described above. The estimated values were compared with measurements carried out with an environmental scanning electron microscope (ESEM). An example of the ESEM measurement is depicted in Fig. 9(a). Unfortunately, the diameter of the template-grown tubes was not uniform. The tubes tended to have a smaller diameter toward the surface of the alumina template (in which they were grown) and a larger diameter in the interior. In other words, the tube's diameter next to its ends was smaller than away from the ends. The variations in diameter were as large as ±20%. For our purposes, we measured the tube's diameter at two to six locations and computed the arithmetic average.

The ionic liquid exhibited essentially no evaporation even under the low pressure (1 torr) of the environmental scanning electron microscope (ESEM). Single drop experiments were carried out with 670 °C and annealed 2000 °C tubes under room conditions (22 °C). For the 670 °C tubes, the flow measurements gave an estimate of the tube radius a as 177±6 nm in good agreement with the SEM-measured radius of 180±10 nm. For annealed 2000 °C tubes, the flow measurements provided an estimate of the effective tube radius $a \sim 152\pm 11$ nm while the SEM measurements gave $a \sim 181\pm 2$ nm. If we assume that the 670 and 2000 °C tubes had similar effective radii, the experiments would suggest that the flow rate in the 2000 °C annealed tube was 1.8 times larger than in the 670 °C amorphous tube. Given the tubes' nonuniformity, the above discrepancy may very well have resulted from experimental error rather than a fundamental difference in the flow behavior in the amorphous and graphitized tubes.

A larger set of experiments was carried out with glycerin. A comparison of the hydraulic estimates of the tube's effective radii (dark bars) and the SEM measurements (light bars) for the 670, 1850, and 2000 °C tubes are recorded, respectively, in Figs. 9(b)–9(d). The abscissa identifies individual tubes and the ordinate shows the estimated a value from the experiment. Multiple experiments were conducted with the same nanotube. The scatter of the radii estimates was smaller than 15% and is documented with error bars in the figure. The single and double drop experiments yielded similar estimates for the tube radii. In all cases, the tubes' radii, estimated from the hydraulic experiments, were smaller than the ones measured with the SEM. On average, the hydraulically determined radii of the 670, 1850, and 2000 °C tubes were, respectively, 77%, 84%, and 75% of the SEM-measured radii of the same tubes.

The hydraulic estimates of the tubes' radii were consis-

Downloaded 14 Mar 2007 to 165.123.34.86. Redistribution subject to AIP license or copyright, see http://pof.aip.org/pof/copyright.jsp

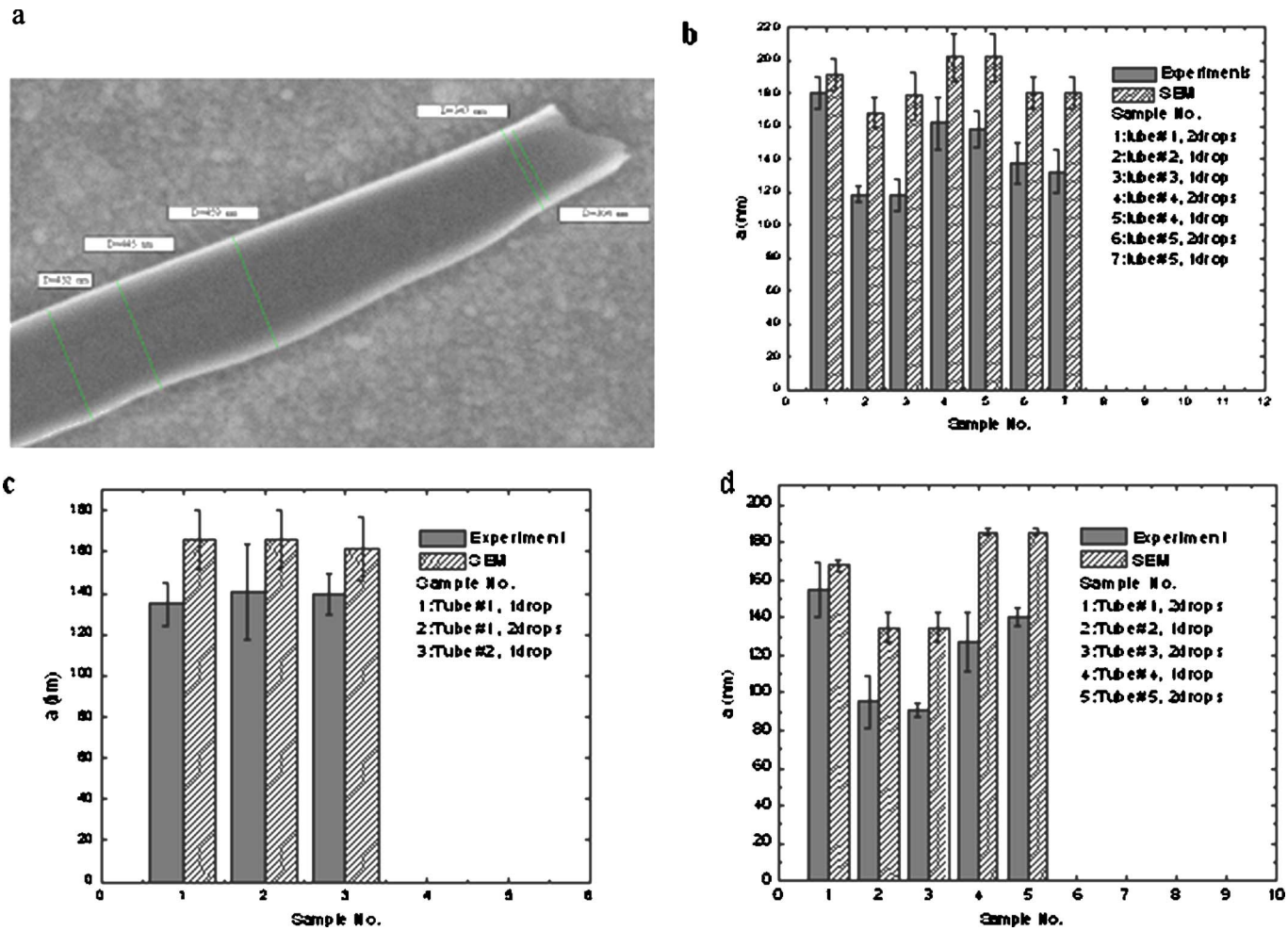

FIG. 9. SEM image of a carbon nanopipe (a). Hydraulically estimated (dark bars) and SEM-measured (shaded bars) radii of the 670 °C (b), 1850 °C (c), and 2000 °C (d) nanopipes. The working fluid is glycerin.

tently smaller than the SEM measurements. Although the above difference is well within the experimental uncertainty, the consistency of the data suggests some underlying physics. We speculate that the SEM data overestimates the effective diameter of the tube because, due to van der Waals interactions between the tube and the substrate on which the tube rests, the tube flattens somewhat and assumes an elliptical cross section. In other words, $a_{\|} > a_{+}$, where $a_{\|}$ and a_{+} are, respectively, the tube's chord lengths parallel and normal to the surface. With the SEM, we can only determine $a_{\|}$. Indeed, Ruoff *et al.*[20] showed with TEM images that van der Waals forces deform multiwalled nanotubes (MWNTs) when they come in contact with each other. We observed similar behavior with our CVD-grown nanopipes.[14] Using AFM observation with continuum mechanics and molecular-dynamics calculations, Hertel *et al.*[21] showed that the deformation due to van der Waals forces between substrate and nanotubes could be significant.

VI. DISCUSSION AND CONCLUSIONS

We described a simple technique that allows us to induce pressure-driven fluid motion through individual nanotubes while simultaneously monitoring the flow rate and pressure drop across the tube. The technique is particularly attractive when carrying out experiments with ionic liquids that do not experience any evaporation. In that case, the experiments can be carried out inside a SEM chamber with nanosize droplets. Thus, the technique can be used in conjunction with much smaller tubes than the ones described in this paper. Unfortunately, we were not able to carry out such experiments with a SEM for lack of an appropriate instrument that allows drop manipulation while the sample is inside the vacuum chamber of the electron microscope.

In most prior investigations addressing fluid flow through nanotubes, researchers carried out the measurements with membranes consisting of many tubes. By necessity, the experimenters measured quantities averaged over tubes with various sizes.[12,13] In contrast, the experimental technique described herein can be used with a single tube.

Of significant current interest is the determination of whether highly confined fluids behave differently from their macroscopic counterparts. In our experiments with the ~300 nm diameter amorphous and graphitized tubes, we did not observe significant deviations from classical behavior. Our estimates of the effective tube radii using accepted values of viscosity were consistent with radii values measured with SEM.

Downloaded 14 Mar 2007 to 165.123.34.86. Redistribution subject to AIP license or copyright, see http://pof.aip.org/pof/copyright.jsp

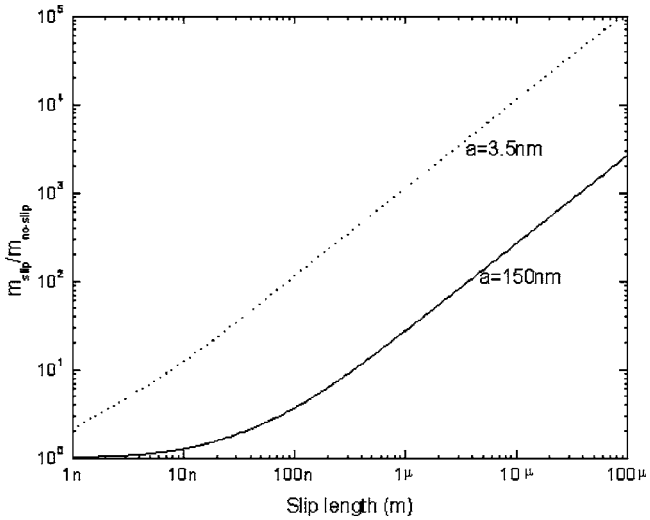

FIG. 10. The ratio of flow rates in the presence and absence of slip as a function of the slip length when the tube radius is 3.5 nm (dotted line) and 150 nm (solid line).

In contrast, recent experiments with multiwalled carbon nanotubes (MWNT) with diameters ranging from 1.3–2 nm (Ref. 13) to 7 nm (Ref. 12) have resulted in "superfluidity"—flow rates 4–5 orders of magnitude higher than predicted with the classical theory, which assumes nonslip at solid boundaries. Often, when the flow rate is higher than expected, the results are characterized in terms of the slip length λ. In other words, classical theory would predict the observed flow rate if the tube's radius were $a+\lambda$ instead of a. Based on their experiments, Majumder *et al.*[12] and Holt *et al.*[13] estimate, respectively, slip lengths ranging from 3–70 μm and 0.1–1.4 μm. The effect of the slip length on the flow increases as the tube's radius decreases. Figure 10 depicts on a log-log scale the ratio of the flow rates in the presence and absence of slip as a function of the slip length when the tube's radius is 3.5 nm (dotted line) and 150 nm (solid line). When $\lambda=3$ μm, one would expect to see, respectively, ~3000- and ~40-fold increases in the flow rates for the tubes with radii of 3.5 and 150 nm. In our experiments, the measured flow rates were close to the theoretical predictions and certainly did not exceed the theoretical predictions by a factor of 40. Thus, our experimental observations do not confirm the experiments of Majumder *et al.*[12] and Holt *et al.*[13]

It is possible, however, that both differences in the tubes' sizes and their material properties prevented us from duplicating the experimental measurements of Majumder *et al.*[12] and Holt *et al.*[13] It is conceivable that superfluidity is caused by confinement and not surface effects, and therefore the theory that we used to predict the flow rate as a function of the slip length is not applicable. It is interesting to note, however, that Raviv *et al.*[22] carried out high precision experiments with a surface force apparatus and did not observe significant deviations between the effective and macroscopic viscosities even when the gap between the confining plates was as small as 0.5 nm. Another possible reason for the difference between our experimental observations and those of Majumder *et al.*[12] and Holt *et al.*[13] is the difference in the surface properties. Although both the authors of Refs. 12 and 13 and ourselves experimented with graphitic tubes, our graphitized tubes contained imperfections.

ACKNOWLEDGMENTS

This work was supported, in part, by the National Science Foundation through Grants No. NSF-NIRT 0210579 and No. NSF-CBET 0609062 and by the Nano/Bio Interface Center (Grant No. NSF NSEC DMR-0425780).

[1] J. M. L. Poiseuille, "Experimental investigations upon the flow of liquids in tubes of very small diameters, sciences mathematiques et physiques" (translated from French to English by E. C. Bingham) (1846), Vol. 9.
[2] J. N. Pfahler, "Liquid transport in micron and submicron size channels," Ph.D. dissertation, University of Pennsylvania (1992).
[3] J.-T. Cheng and N. Giordano, "Fluid flow through nanometer-scale channels," Phys. Rev. E **65**, 031206 (2002).
[4] N. V. Churaev, V. D. Sobolev, and A. N. Somov, "Slippage of liquids over lyophobic solid surfaces," J. Colloid Interface Sci. **97**, 574 (1984).
[5] R. Pit, H. Hervet, and L. Leger, "Direct experimental evidence of slip in hexadecane: Solid interfaces," Phys. Rev. Lett. **85**, 980 (2000).
[6] Y. Zhu and S. Granick, "Rate-dependent slip of Newtonian liquid at smooth surfaces," Phys. Rev. Lett. **87**, 096105 (2001).
[7] K. B. Migler, H. Hervert, and L. Leger, "Slip transition of a polymer melt under shear stress," Phys. Rev. Lett. **70**, 287 (1993).
[8] V. S. J. Craig, C. Neto, and D. R. M. Williams, "Shear-dependent boundary slip in an aqueous Newtonian liquid," Phys. Rev. Lett. **87**, 054504 (2001).
[9] C. Cottin-Bizonne, S. Jurine, J. Crassous, F. Restagno, and E. Charlaix, "Nonorheology: An investigation of the boundary condition at hydrophilic and hydrophobic interfaces," Eur. Phys. J. E **9**, 47 (2002).
[10] D. C. Tretheway and C. D. Meinhart, "Apparent fluid slips at hydrophobic microchannel walls," Phys. Fluids **14**, L9 (2002).
[11] H. H. Bau, S. Sinha, B. M. Kim, and M. Riegelman, "Fabrication of nanofluidic devices and the study of fluid transport through them," Proc. SPIE **5592**, 201 (2005).
[12] M. Majumder, N. Chopra, R. Andrews, and B. J. Hinds, "Nanoscale hydrodynamics: Enhanced flow in carbon nanotubes," Nature (London) **438**, 7070 (2005).
[13] J. K. Holt, H. G. Park, Y. Wang, M. Stadermann, A. B. Artyukhin, C. P. Grigoropoulos, A. Noy, and O. Bakajin, "Fast mass transport through sub-2-nanometer carbon nanotubes," Science **312**, 5776 (2006).
[14] M. P. Rossi, H. Ye, Y. Gogotsi, S. Babu, P. Ndungu, and J. C. Bradley, "Environmental scanning electron microscopy study of water in carbon nanopipes," Nano Lett. **4**, 5 (2004).
[15] D. Mattia, M. P. Rossi, B. M. Kim, G. Korneva, H. H. Bau, and Y. Gogotsi, "Effect of graphitization on the wettability and electrical conductivity of CVD-carbon nanotubes and films," J. Phys. Chem. B **110**, 20 (2006).
[16] D. Mattia, H. H. Bau, and Y. Gogotsi, "Wetting of CVD carbon films by polar and nonpolar liquids and implications for carbon nanopipes," Langmuir **22**, 1789 (2006).
[17] B. Kim, S. Sinha, and H. H. Bau, "Optical microscope study of liquid transport in carbon nanotubes," Nano Lett. **4**, 2203 (2004).
[18] B. M. Kim, S. Qian, and H. H. Bau, "Filling carbon nanotubes with particles," Nano Lett. **5**, 5 (2005).
[19] J. Happel and H. Brenner, *Low Reynolds Number Hydrodynamics* (Martinus Nijhoff, The Hague 1983).
[20] R. S. Ruoff, J. Tersoff, D. C. Lorents, S. Subramoney, and B. Chan, "Radial deformation of carbon nanotubes by van der Waals forces," Nature (London) **364**, 514 (1993).
[21] T. Hertel, R. E. Walkup, and P. Avouris, "Deformation of carbon nanotubes by surface van der Waals forces," Phys. Rev. B **58**, 20 (1998).
[22] U. Raviv, P. Laurat, and P. Klein, "Fluidity of water confined between subnanometer films," Nature (London) **413**, 6851 (2001).

Downloaded 14 Mar 2007 to 165.123.34.86. Redistribution subject to AIP license or copyright, see http://pof.aip.org/pof/copyright.jsp